

CASE STUDY

The last 40,000 years of a floodplain area (Tisza, Hungary) comparative case study of ^{14}C and OSL methods

Titanilla G. Kertész^{1,4} , Katalin Hubay¹, Botond Buró¹ , A. J. Timothy Jull^{1,5}, Andrea Mindszenty², György Sipos³, Tamás Bartyik³ and Mihály Molnár¹ 

¹Isotope Climatology and Environmental Research Centre, Institute for Nuclear Research H-4032, Bem str. 18/c, Debrecen, Hungary, ²Eötvös Loránd University, Department of Physical and Applied Geology H-1117, Pázmány Péter str. 1/a, Budapest, Hungary, ³Szeged University, Department of Physical Geography and Geoinformatics H-6722, Egyetem str. 2-6, Szeged1, Hungary, ⁴University of Debrecen, Doctoral School of Earth Sciences H-4001, Egyetem str. 1, Debrecen, Hungary and ⁵University of Arizona, Department of Geosciences and AMS Laboratory, Tucson, Arizona, USA

Corresponding author: Titanilla G. Kertész; Email: kertesztitanilla@atomki.hu

Received: 10 June 2024; **Accepted:** 25 June 2024; **First published online:** 31 March 2025

Keywords: Jászság Basin; OSL; oxbow; radiocarbon AMS dating; Tisza River

Abstract

To investigate the environmental history of the Tisza River (Hungary), we applied ^{14}C and OSL dating methods for five parallel, neighboring cores from the flood plain area (Jászság Basin). Four major sedimentary layers were identified: meadow soil on the top (S1); silty-clay (S2); clayey-silt (S3) section; and fine sand (S4). ^{14}C and OSL data were integrated into a synthetic age-depth model using the BACON software package. Formation of the S1 layer (depth: 0–1.0 m) falls in the Holocene, up to 10 kyrs cal BP, with moderate sedimentation rate (100 yr/cm aAR). The S2 layer (1.0–8.0 m depth) represent the entire Last Glacial to Upper Pleniglacial period (19–27 kyrs cal BP), with a much faster sedimentation (20 yr/cm aAR). The S3 section (8.0–17.0 m) represents a longer period (27–45 kyrs cal BP) with similar sedimentation rate (19 yr/cm aAR) as S2. These clayey silt layers fall into the Late Pleistocene/Middle Pleniglacial period, a period of nearly 18 kyrs of sedimentation resulting ~9 m thick sediment. Our study delivered some new and important details about the surface evolution of the investigated Tiszasüly area. A missing part of about 10 kyrs period (between 10–19 kyrs cal BP) was revealed in the investigated synthetic cores.

1. Introduction

Geochronology carries essential information for paleoclimatic and paleoenvironmental reconstruction. The estimated ages provided by various dating methods and techniques allow deducing past environmental conditions and their development. There are more and more studies published, that combine radiocarbon dating and optically stimulated luminescence (OSL) results (Buró et al. 2016; Crombè et al. 2012; Kiss et al. 2012, 2015; Miao et al. 2016; Nian et al. 2017; Újvári et al. 2014, 2016). Although several methods are available to study the chronology, the suspected age interval as well as the quality and quantity of accessible materials may influence the selection of appropriate procedures.

In a flood-plain environment, the dynamics of landform formation might be more variable/rapid than in other areas. Nevertheless, the evolution of river channels and flood plains over time have great significance in the study of environmental change, so this has received considerable international attention (Bertalan et al. 2019; Shen et al. 2015; Szabó et al. 2012). Sediments of different ages from distant areas can also be transported to a flood plain by the flood events, which is why investigating the chronology of flood plains could be challenging for ^{14}C dating. In this study, along with ^{14}C dating, we also applied OSL dating technique to verify the ^{14}C based chronology to gain a more reliable age profile.



However, the correlation between these two different techniques is greatly influenced by the sample material (Miao et al. 2016). For example, Újvári et al. (2014, 2016) have published calibrated radiocarbon ages (gastropod and charcoal ages) that are much older than the OSL results for the Dunaszekcső loess sequence, which raises methodological questions.

Based on earlier hypotheses, hundreds of meters of Late Quaternary sediments might have been deposited in this area (Franyó 1992; Gábris 2001, 2002; Nádor et al. 2003; Rónai 1985; Timár 2003; Vandenberghe et al. 2018). It has been suggested that the thickness of Holocene sediments alone should be 30–40 m on top of the sediment profile (Kuti and Kőrössi 1989).

Using absolute dating methods, we wanted to support and verify previous opinions regarding this area, which were based largely on geophysical, geomorphological and sedimentological observations. Only scattered reports of previous stratigraphic studies carried out with absolute dating are available from this area. Based on these, the abandoned river channels were created in the last 4–29 kyr ^{14}C years cal BP in the surroundings of the Tisza, Sajó and Bodrog, from the LGM to the new Holocene. In many cases, the estimation of the formation age of individual developmental stages and surfaces can only be linked indirectly with the results of ^{14}C measurements carried out in more distant areas.

1.1 Research objectives

In this study, we aim to interpret our sediment dating results and fit them to the Late Pleistocene/Holocene history of the Jászság Basin, comparing them to the already published literature (Kuti and Kőrössi 1989).

To achieve a reliable age-depth model, we replicated the dating of sediments in the middle section of the river Tisza with more advanced AMS radiocarbon dating, which involved the preparation of different fractions of soil organic matter and analyses of very small (< 0.1 g) fossil remains (gastropods and charcoal fragments).

Radiocarbon dating of soils is mainly used for the chronology of soil development. In archaeological and environmental archaeological studies, if there are no fossil remains available for ^{14}C measurements, there are a number of examples in the literature of the applications of bulk sediment ^{14}C ages, where the reservoir effect can be taken into account (Harrison 1996; Wang et al. 1996; Brock et al. 2010). However, dating of bulk samples, particle size fractions, and organic matter fractions from soil samples has been carried out with only small and varying degrees of success in the last 20–25 years (Chichagova and Cherkinsky 1993; Hemingway et al. 2019; Scharpenseel and Becker-Heidmann 1992; Tamm and Östlund 1960; Trumbore 2000; Wang et al. 1996). The steady-state apparent radiocarbon age (reservoir-age) of living soils can be very different (from hundreds to thousands of ^{14}C years cal BP) according to the geological location. This depends on the climate, parent material, precipitation, chemical environment, flora and many other parameters (Buró et al. 2019; Molnár and Svingor 2011; Novák et al. 2018; Scharpenseel and Becker-Heidmann 1992; Tóth et al. 2018; Wang et al. 1996). The ^{14}C age of the soil organic carbon (SOC) pool is subject to many processes affecting the vertical and horizontal pattern of carbon in the soil and exchange between soil and biosphere (Doetterl et al. 2016; Wiaux et al. 2014). Various sources of carbon can modify the ratio of modern and older carbon in the composition of SOC (Hales et al. 2012). An increasing age of soil organic carbon that parallels increasing distance from the soil surface is expected, since most sources of new carbon from roots exudation (Doetterl et al. 2016; Novák et al. 2018).

2. Study area

The research area is located in the Central Tisza basin of the Great Hungarian Plain, the Jászság Basin, which is one of the unevenly sinking basins of the Great Plain (avg. 3 mm/yr since the late Miocene) (Joó 1992; Timár et al. 2005). In terms of its tectonics, it is formed by N-S-striking, young normal and strike-slip faults (deforming late Miocene, Pliocene, Quaternary layers, inactive today) normal and

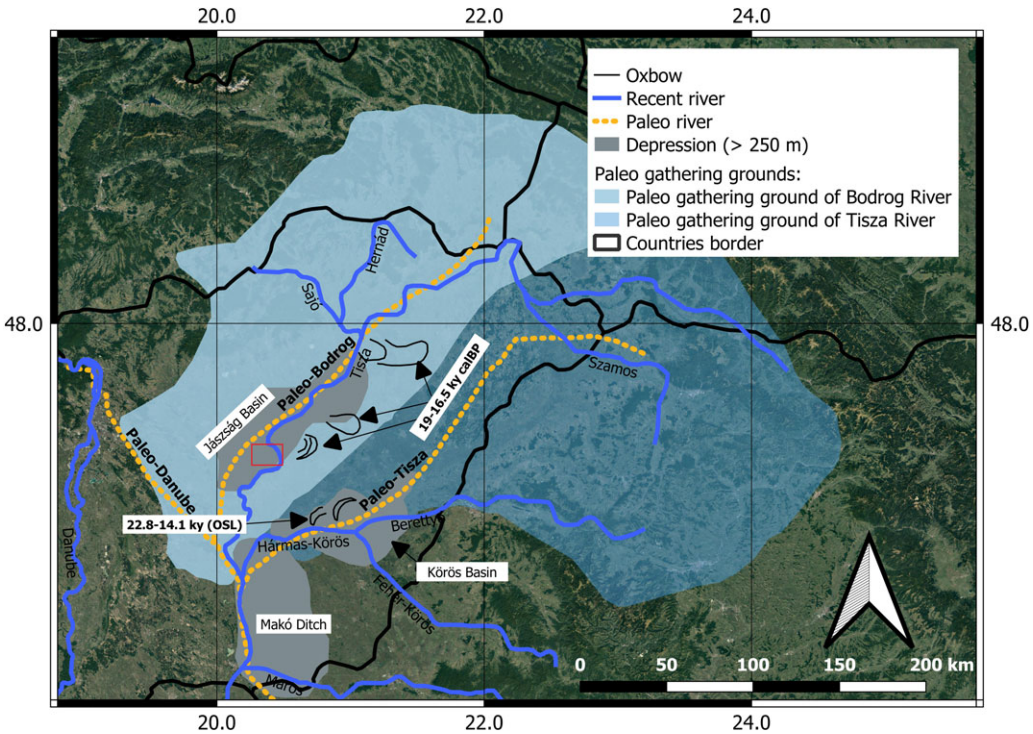


Figure 1. Hypothetical watershed and river channels (black dashed line) of the Paleo-Tisza, “Paleo-Bodrog”, Paleo-Danube and the present rivers Tisza (red square is the study area) and Danube. The age data shown in the figure are those of the subsurface and surface traces of the former abandoned meanders/oxbows (after Gábris and Nádor 2007).

laterally displaced faults (Horváth and Tari 1999; Horváth et al. 2006). The Great Hungarian Plain is one of the most beautiful examples of alluvial plains, which shows exceptionally small—sometimes less than 100 m—elevation differences. Sediments deposited mainly by running water in the Quaternary are responsible for its formation (Gábris 2002; Gábris et al. 2001; Nádor et al. 2003, 2007; Thamóné-Bozsó et al. 2002; Timár et al. 2005; Vandenberghe et al. 2016, 2018).

During the Pleistocene, the area of the Jászság Basin continuously sank, as a result of which riverine recharge was intense (Miháltz 1967). Total thickness of the sediments deposited at that time exceeds 300 m.

The research area lies in the past flood plain of the river Tisza (altitude ~85–90 mBf sea level above the Baltic Sea in meters). Its morphology has been shaped by the meandering Tisza and Zagyva Rivers, thus the surface is now covered by a rich network of abandoned river channels and oxbows.

The Paleo-Tisza flowed across the Nyírség alluvial fan in the direction of the Érmellék-Berettyó Rivers during the Pliocene (Borsy 1954; Borsy and Félegyházi 1982; Sümeghy 1944). During the late Pleistocene, by avulsion, the river Tisza was able to reach its final position with the sinking of the Bodrogtköz and the Bereg-Szatmári-plain (Borsy 1954, 1989; Nagy et al. 2007). The Tisza is now further to the west than earlier and reached its present-day path between about 14 kyr (Gábris and Nádor 2007) and 16–18 kyrs (Timár et al. 2005; Vandenberghe et al. 2016) ago. There might have been several meander cutoffs about 14 kyrs ago (or 16–18 kyrs ago) until the river finally shifted to its current position.

Based on the currently available age and climatic data, Gábris (2002) created a triaxial paleohydrological model for the late Pleistocene (Figure 1) (Gábris 2002). They suggest that there was a third river, the “Paleo-Bodrog,” with notable water output next to the Paleo-Tisza and

Paleo-Danube. The supposed sediments of the “Paleo-Bodrog” were found by Nagy et al. (2005) below the present-day channel of the river Tisza. Figure 1. shows the age data of the subsurface and surface meander traces (Gábris and Nádor 2007; Nádor et al. 2003, 2007). According to Gábris and Nádor (2007) 5 kyr ago, at the Atlantic/SubBoreal boundary, there was another change due to tectonics (Gábris 2011).

As a consequence of tilting of the Great Hungarian Plain, the meandering trail of the river Tisza gradually shifted westward (Mike 1975).

During the Quaternary, major changes in the hydrological network were determined by high-frequency and high-amplitude instability of the climate manifested as alternating interglacial (warmer) and glacial (colder) periods. At the time of glacial periods, both shorter or longer high intensity colder (stadial) and warmer (interstadial) periods can be identified (Emiliani 1955; Kretzoi and Pécsi 1982a, 1982b; Penck and Brückner 1901–1909; Shackleton 1967; Shackleton and Opdyke 1973). During the Holocene, the climate has been relatively more stable, but lower-amplitude climatic oscillations have still occurred.

The research area, together with the whole Carpathian Basin, was part of the periglacial belt during glacial periods of the Pleistocene, so contiguous ice cover affected the land surface only in the mountainous regions to the north. During the glacial period, the lowland areas were characterized by an extremely continental climate, with a high level of drought, which resulted in the preservation of records of aeolian processes, such as wind erosion, loess deposition, wind-blown sand (Fábián et al. 2000; Gábris 2003; Horváth et al. 2007; Jámboor 2002). During interglacial warming, rainfall increased and the surface water and groundwater from the melting of the snow cover of the surrounding mountains (Carpathian Mountains) resulted in higher water abundance, thus facilitating alluvial sedimentation and also soil formation even on higher elevated grounds and floodplains.

Because sedimentation in this near-floodplain environment has had highly variable dynamics, and some major floods or other erosional effects may even have removed parts of the sequence, we may also have to consider a possible *hiatus* in the record. In addition, our small study area was very likely an oxbow section, with a low accumulation rate.

3. Methods

Five shallow boreholes (avg. depth 19–20 m), were drilled for industrial purposes in the Jászság Basin 2.5–3 km (in 2016) away from the main channel of the river Tisza (near Tiszasüly) (Figure 2). The core (core diameter 70 mm and double tube core barrel 101 mm diameter casing) was obtained using a B1A type Wirth drilling rig.

The selection of samples from each stratum in our study was driven by our wish to check the validity of the assumption of previous scholars (Kuti and Kőrössy 1989; Rónai 1985), according to which the entire stratum (~20 m) was supposedly accumulated in the course of the Holocene, over the past 11,200 years. We wanted to examine this presumption by an improved measuring technique. In cases where there was a sharp lithological change in the sections, which was probably related to major developmental and/or climatic events and changes, we also collected OSL samples in parallel with ¹⁴C sampling. Thus, an independent method was used to check the chronology of events. ¹⁴C and OSL results of 5 parallel, neighbouring cores were compared for a flood plain area to provide independent estimates of the sediment age. In this way, we examine the effect of the physical placement of the boreholes on the different age results, as well. We aimed to compare data from the five parallel boreholes, including the stratigraphy and to scrutinize the lithological changes in the stratigraphy for possible traces of eventual significant past environmental or climatic shifts related to the lithohorizons.

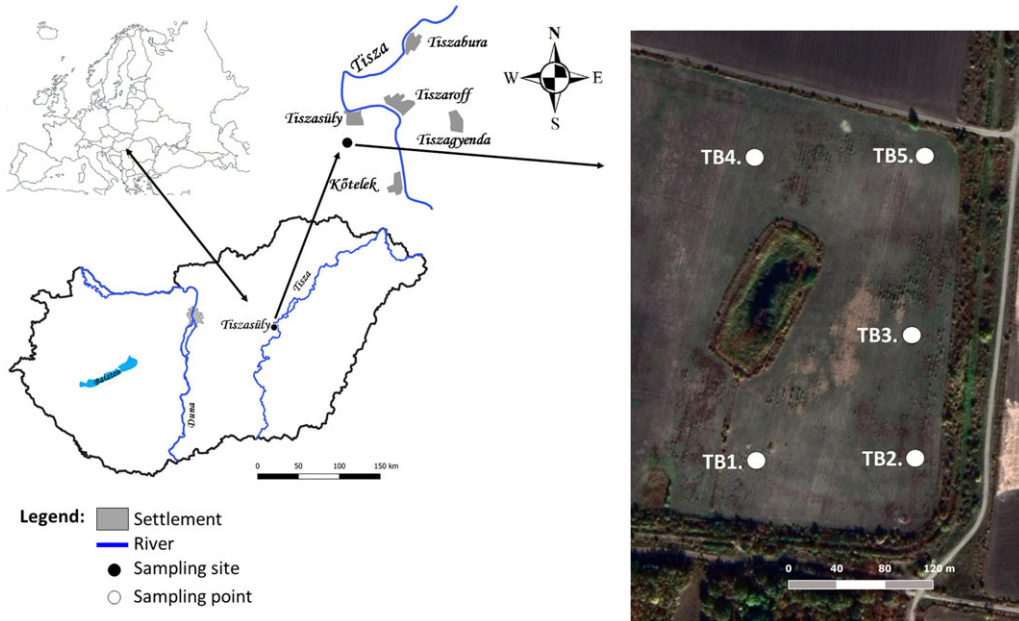


Figure 2. Location of the sampling site in the Carpathian Basin.

3.1. Description of the cores and sampling

The description and measurement type of the investigated beds of the 5 parallel cores (TB-1 to TB-5, taken as representative of the Tizasüly borehole cores) is summarized in Table 1. The material from the drill-cores was subdivided into 4 major sedimentary layers (S1 to S4), according to lithostratigraphic observations, namely meadow soil on the top (S1-A, B, C); silty-clay (S2) below; a clayey-silt (S3) section further below; and finally, a fine-sand (S4) at the bottom of the hole (Figure 3). The fine-sand (S4) layer is obviously older age than 40 kyrs, thus it is out of the scope of our study, therefore we did not examine it any further.

On the top of the sequences (S1, Solonetz meadow soil), the dark brownish gray (Munsell 2.5Y-3/3) blocky structured humic layer of about 1–1.5 m thickness belongs to the current alkaline soil (Figure 3). Comparative bulk ^{14}C samples were taken from the upper meadow soil layer (S1) of the 5 parallel drills, preferably from soil depth horizons of the same depth. We separated the top soil horizon (recent top meadow soil, S1-A), the middle level (S1-B) and finally the bottom meadow soil (sub-level, S1-C) in the sequence.

Below that, the underlying layer (S2) is a 5–8 m thick yellow gray (Munsell 10YR-6/6) gleyic, mottled, silty-clay formation with Fe concretions and rhizoconcretions. It is a carbonate-sulphate-pedocal-solonetz type soil-sedimentary complex. Its unusual thickness is apparently due to the aggradation of the flood plain. The redox-mottling refers to a past and also present position close to the level of the groundwater-table and is very characteristic of the flood plain environment. During the drilling operations, the actual groundwater-table was around 2 m below the surface. It oscillated with the water level of the river Tisza. The formation displays a non-stationary, at most intermittent hydromorphy.

From the upper level of the silty-clay (S2), below the uppermost meadow soil, close to the boundary between the meadow soil and the silty layer (mean depth: 1.02 ± 0.2 m), there was a large amount of snail shells, CaCO_3 concretions (see Table 1) in almost every borehole, so it seemed appropriate to take ^{14}C samples also here.

Table 1. Specific observations about the layers from which ^{14}C /OSL samples were collected

Sample name	Core code	Depth (m)	Specific observations about the sampled horizons (soil) and layers
Meadow soil (solonetz) (S1-A,B,C) (0.0–1.5 m)	TB-1 to 5	0.0–0.2	Recent surface
		0.4–0.8	Gypsum precipitates, 0.2–1 cm CaCO_3 concretions, granular soil structure, clayey
		0.8–1.2	Sulphate precipitates, animal burrows, CaCO_3 concretion
Silty-clay (S2) (1.5–8.0 m)	TB-3	1.0–1.2	Fe-Mn mottles, <1 cm calcite crystals, snails
	TB-4	1.5–1.7	Silt, gley spots Mn-mottles, CaCO_3 concretion, shell and entire snail
	TB-3	1.7–2.3	Gley spots, small Fe-Mn mottles and snails, the silt content increases
	TB-5	1.8–2.0	Soil structure, gleyification, lime, many CaCO_3 concretion, snail
	TB-2	2.0–2.2	Silty, gleyification, Fe-Mn mottles, mildly micaceous, shell and entire snail
	TB-1	2.0–2.3	Snail, 1.5–2 cm lime concretion
	TB-3	2.6–3.0	Silt, laminate
	TB-1	3.0–3.2	More clay (higher amounts of clay), micaceous, snail
	TB-3	3.5–3.8	Fe-Mn mottles
Clayey-silt (S3) (8.0–18.0 m)	TB-1	8.1–8.5	Clayey, lots of organic detritus, grey laminated
	TB-4	8.4–8.8	Dark brown (Munsell 7.5YR-2/3) peat, muddy, laminated, vivianite
	TB-5	8.6–8.7	Laminated, silty-clay, rhodochrosite
	TB-4	10.8–11.0	Fine sandy, silt, 6 cm shell and many snail fragments
	TB-3	12.3–12.4	>5 cm shells parallel to the bedding plane, snail, blue ochre (11–12 m)
	TB-1	16.6–16.9	Little silt, goethite, rip-up flood-plain clay clasts
Fine sand (S4) (>18.0 m)	All cores	18.0	Downward increasing sand content, CaCO_3 concretion. Its expected age is well over 40 krys, so it was not examined this in more detail.

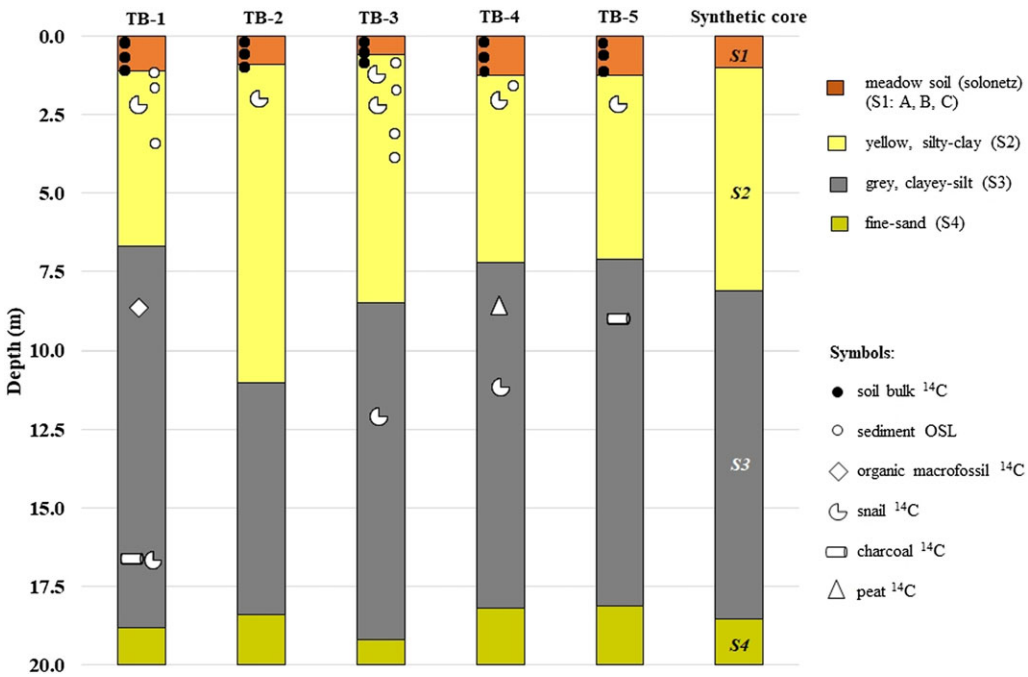


Figure 3. Correlated drilling profiles with sampling points (synthetic core: Compiled for the integrated interpretation of all the measured ages and for a common age-depth model. The boundaries of the individual layers were calculated as the mean of the actual depth of the particular layer(s) in each investigated (TB-1 to TB-5) core. S1-A, B, C: The three levels of the meadow soil horizons (recent top; middle level; sub-level). S2; S3; S4: Levels below the meadow soil layer (silty-clay; clayey-silt; and boundary between the clayey-silt and sandy layer).

Samples from the lithologically distinct levels exhibit significant geochemical characteristics, as the silty-clay (S2) has a weak alkalinity, an organic content of 1.5–1.8%, and a low to medium degree of polymerization of the organics. An exception is the organic matter content of the TB-4 borehole sample taken from the peat layer at 8.5 m (S3 clayey-silt layer), which is extremely rich in organic matter (reaching 10.2%) and is also slightly alkaline. This layer reflects a climatic period that may have resulted in a wetter, more restricted anaerobic environment that favoured the formation of peat. To investigate this more closely, radiocarbon samples were also analysed here. In most cases, the same type of macrofossils was extracted from the same relative depth intervals, making the correlation between parallel cores even more accurate.

The transition from S2 to S3 layers starts from the yellow blocky-structured part (S2), which is significantly different from the underlying dark-gray, laminated part (S3). This visible difference is likely due to a change of the drainage/deposition conditions in the past.

The underlying layer (S3), which is the thickest (9–10 m) part of the sequence, is a dark-gray (Munsell 5GY-4/1, 5Y 4/1, N3) laminated micaceous clayey-silt. While it is structurally sharply separated, its color shows gradual transition from the overlying formation. At the bottom, the appearance of 10–20 cm sand intercalations becomes more frequent. The sediment suggests accumulation under stagnant water conditions, which was probably the result of the filling of an abandoned meander. At the bottom of this section, fine-grained sand was found, likely deposited by the “Paleo-Bodrog” (Cserkész-Nagy 2013; Gábris 2002; Nagy et al. 2005, 2007). The lowest section of S3 was either a swamp represented by a thin layer of peat, or it was an aggradating flood plain. At the deepest point of this section, the peat layer described reflects a swamp-like environment. A dark gray, laminated loamy layer forms the lower part of the sediment here. It is stained with organic matter

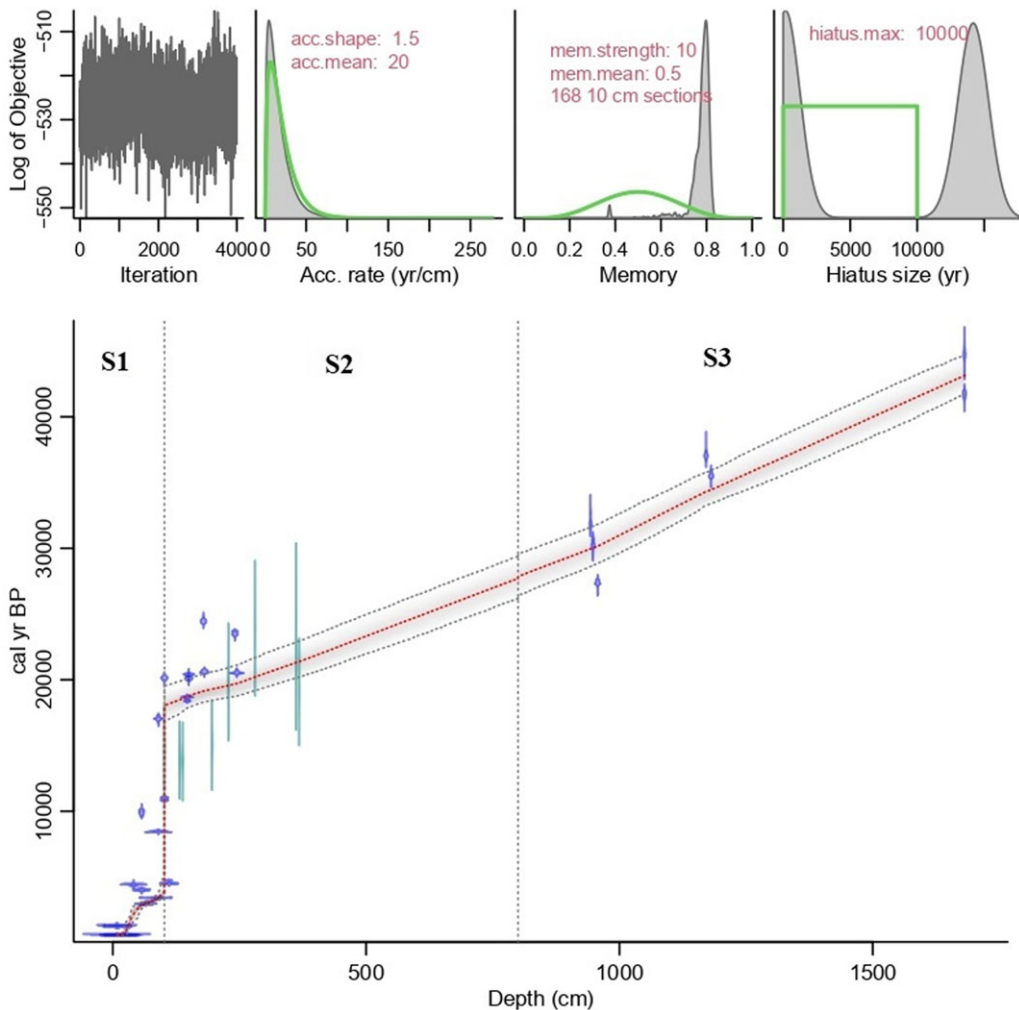


Figure 4. Age-depth model of the whole section of the synthetic core (S1 to S3 layers). The blue symbols are the ^{14}C results and the light green symbols are the OSL results. The vertical dashed lines mark the boundaries of each layer in the model.

suggesting, oxygen poor and reducing depositional environment, resulted by organic decay. These reducing conditions are well-illustrated also by the presence of vivianite and rhodochrosite.

A thick gray fine sand (Munsell 10GY-4/1) layer (S4) appears at the very bottom of all the boreholes (> 18.5 m). It is a clayey, in some parts micaceous, silt and at the depth of 19 m shows a large CaCO_3 -concretion and one limonitic nodule. The originally laminated sedimentary structure is difficult to observe here and the sand content strongly increases downwards. This section is obviously older than 40 kyrs, so we did not examine this section further.

A “synthetic” core sequence was constructed to gain a synthetic model of the cores, which was applied for the integrated interpretation of all the measured ages and for a common age-depth model (see Figures 4–6). In the synthetic sequence, the boundaries of the individual layers were calculated as the mean of the actual depth of the particular layer(s) in each investigated (TB-1 to TB-5) cores (Figure 3, Table 2).

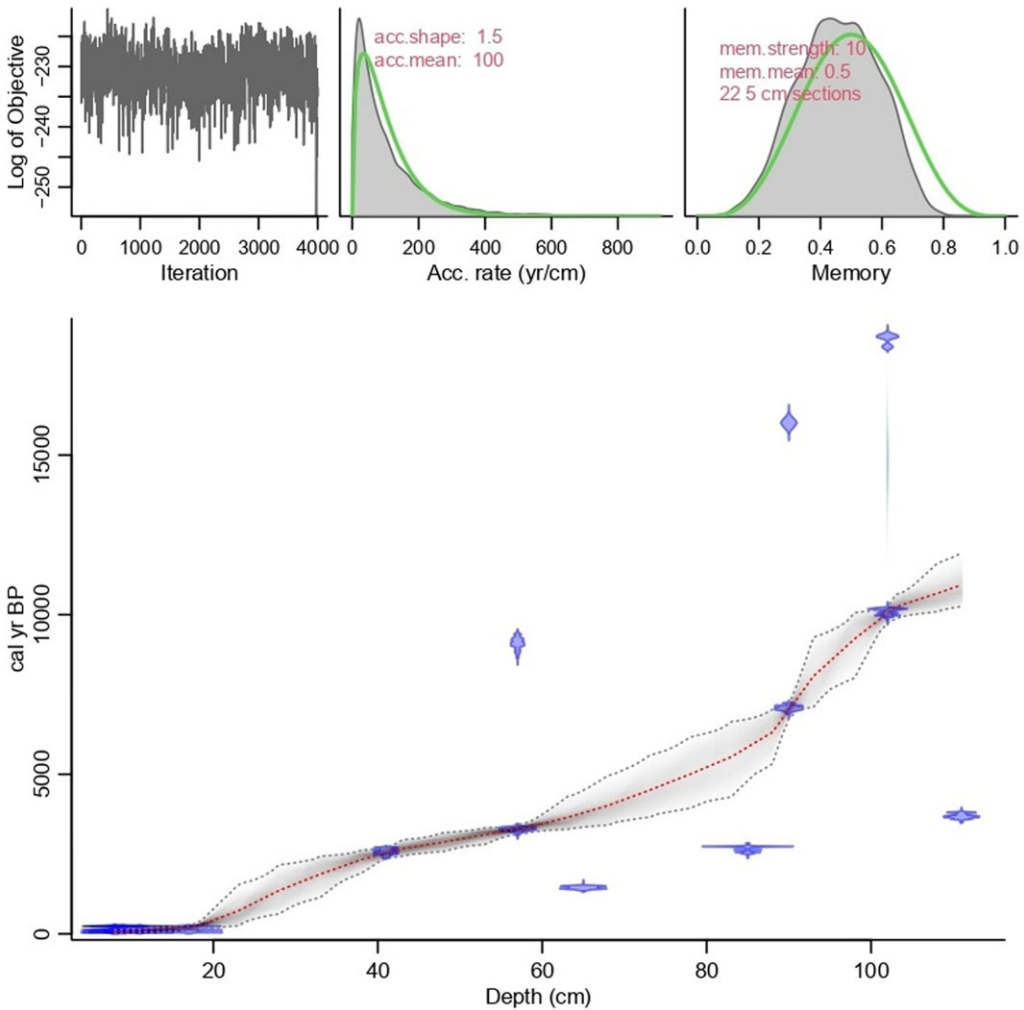


Figure 5. Age-depth model of the Holocene section (SI: A, B, C) of the synthetic core (blue symbols: ¹⁴C results; light green symbols: OSL results).

3.2 Radiocarbon and OSL sample selection

In all cases, we separated macrofossil materials for radiocarbon dating from the floodplain sediments (altogether 9 gastropods, 1 bivalve, 1 sample of peat, 1 macrophyte, and two pieces of charcoal). For later comparison of the results, the samples were selected specifically from stratigraphically-correlated layers. In most cases, the same type of residuals were extracted from the same relative depth intervals from each core, to help more accurate correlation between the parallel cores. Additional sampling points were needed to identify the age of the sharp lithological change between the silty-clay and clayey-silt layers. With this in mind, ¹⁴C samples were taken from above and below this boundary, and also from the lowest sandy section.

Determining the organic matter (SOM: soil organic matter) content, the Walkley-Black method was used (Stefanovits et al. 1999; Van Reeuwijk 1995) of the samples. The color of the sediment samples was described according to the Munsell Soil Color Chart (Munsell 1990). Well-separated boundaries in the sequences below the ground-water level were also sampled. The Solonetz-meadowy type topsoil was sampled at three levels (at the recent surface; at middle level; and at the contact with the

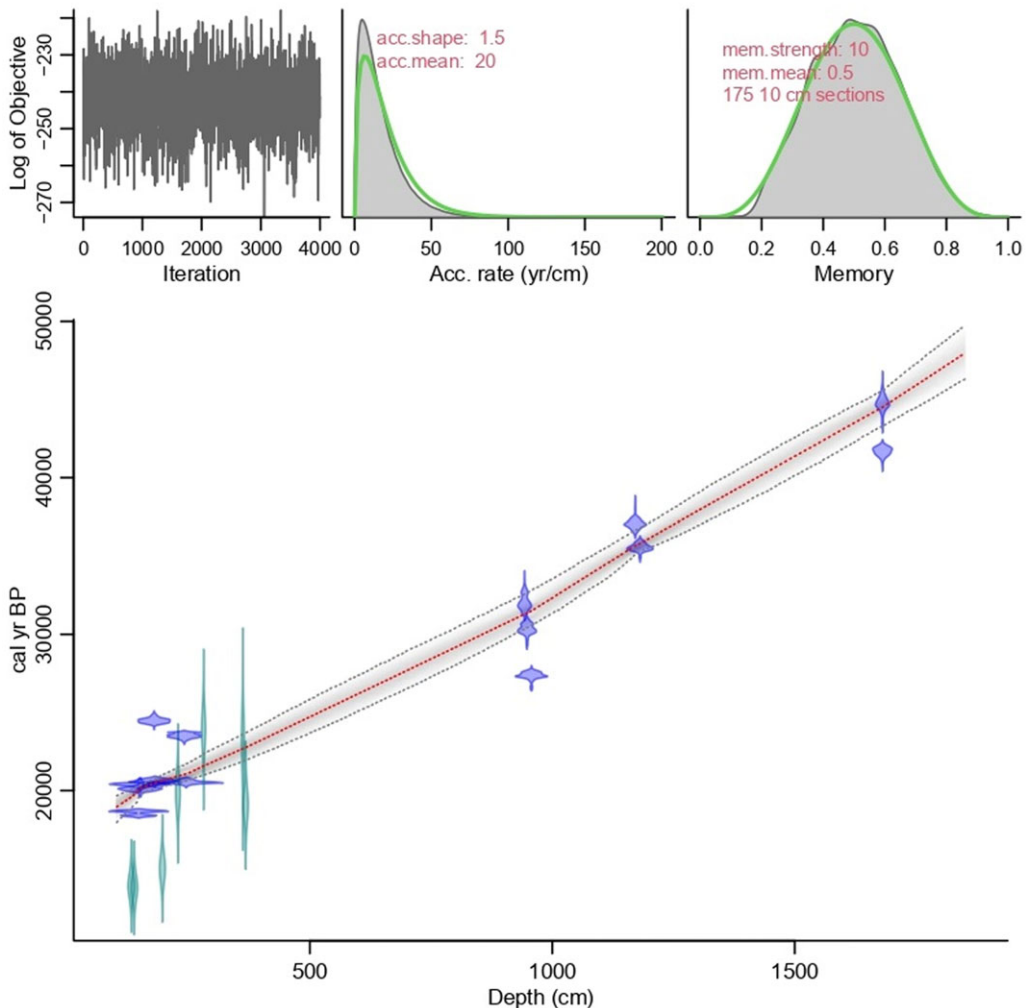


Figure 6. Age-depth model of the Last Glacial; Upper Pleniglacial and Middle Pleniglacial section (S2-S3 layer). (blue symbols: ^{14}C results; light green symbols: OSL results).

yellow-colored silty-clay) down to the ground-water level (1.5-to-2-m depth) with a 10 cm general screw auger. Sediment samples were taken at every 20 cm for radiocarbon dating from soil organic matter. Also, OSL sampling was undertaken, but at slightly greater depth intervals (3–3.5 m) (see Figure 3. for locations of radiocarbon and OSL samples). OSL sampling by using hand drills was performed later than the main drilling campaign, which is why it was not possible to sample the underlying sandy deposits for optical dating.

3.3 OSL analyses

Optically stimulated luminescence (OSL) is a trapped-charge dating method, which can be applied to determine the age of sedimentation, i.e. the last time when the quartz or feldspar grains of the investigated sample were exposed to a sufficient amount of sunlight. However, in fluvial deposits, exposure time may not be long enough to reset or bleach the traps responsible for charge accumulation

Table 2. Summary of radiocarbon and OSL ages of gastropod, bivalve, charcoal, bulk SOC soil and sediment

Sedimentary layers, texture	Cores code (sample depth, m) dated material/fraction	Depth in the synthetic core* (m)	AMS/OSL Lab code	Conv. ¹⁴ C (yr BP [1 σ])	Cal BP ¹⁴ C (yr, 2 σ)/ OSL age (yr) ^a	C yield (m/m %)
<i>Meadow soil horizons (depth: from 0.00 to 1.02 m)</i>						
Recent top (S1-A)	TB-4 (0.0–0.2) SOC H-fraction	0.08	DeA-10348	686 ± 23	Modern ^x	0.56
	TB-5 (0.0–0.2) SOC H-fraction	0.08	DeA-10354	1467 ± 26	Modern ^x	0.56
	TB-1 (0.0–0.2) SOC H-fraction	0.09	DeA-10330	1290 ± 23	Modern ^x	0.54
	TB-2 (0.0–0.2) SOC H-fraction	0.11	DeA-10336	604 ± 22	Modern ^x	0.55
	TB-3 (0.0–0.2) SOC H-fraction	0.17	DeA-10342	621 ± 23	Modern ^x	0.46
Middle level (S1-B)	TB-5 (0.4–0.6) SOC H-fraction	0.41	DeA-10356	3965 ± 29	2434–2741 ^x	0.40
	TB-2 (0.4–0.6) SOC H-fraction	0.57	DeA-10338	3678 ± 31	3180–3373 ^x	0.22
	TB-4 (0.6–0.8) SOC H-fraction	0.57	DeA-10350	8847 ± 102	8774–9429 ^x	0.08
	TB-1 (0.6–0.8) SOC H-fraction	0.65	DeA-10332	2853 ± 25	1382–1534 ^x	0.32
	TB-3 (0.4–0.6) SOC H-fraction	0.85	DeA-10344	3204 ± 26	2508–2768 ^x	0.39
Sub-level (S1-C)	TB-5 (1.0–1.2) SOC H-fraction	0.90	DeA-10358	7653 ± 37	6956–7239 ^x	0.29
	TB-4 (1.0–1.2) SOC H-fraction	0.90	DeA-10352	14002 ± 72	15773–16246 ^x	0.13
	TB-1 (1.0–1.2) SOC H-fraction	1.02	DeA-10334	16662 ± 85	18436–18822 ^x	0.09
	TB-1 (1.0–1.2) sediment	1.02	OSZ 1613	–	14780 ± 820	–
	TB-2 (0.8–1.0) SOC H-fraction	1.02	DeA-10340	9582 ± 41	9921–10235 ^x	0.18
	TB-3 (0.6–0.8) SOC H-fraction	1.11	DeA-10346	4054 ± 31	3590–3827 ^x	0.29
<i>Boundary between Meadow soil and Silty layer (mean depth: 1.02 ± 0.2 m)</i>						
Silty-clay layer (S2)	TB-4 (1.5–1.7) sediment	1.32	OSZ 1606	–	13890 ± 740	–
	TB-3 (1.1–1.2) sediment	1.38	OSZ 1609	–	13780 ± 750	–
	TB-3 (1.1–1.2) gastropod fragment	1.47	DeA-7450	15326 ± 55	18450–18750	11.6
	TB-4 (1.5–1.7) gastropod fragment	1.50	DeA-14632	16878 ± 63	20130–20560	12.0
	TB-4 (1.5–1.7) snail (<i>Pupilla sp.</i>)	1.50	DeA-14633	16637 ± 68	19850–20300	11.1
	TB-2 (2.0–2.2) snail (<i>Pupilla sp.</i>)	1.79	DeA-7449	20380 ± 77	24210–24850	10.3
	TB-5 (1.8–2.0) snail	1.81	DeA-14630	17056 ± 67	20350–20790	11.5
	TB-3 (1.6–2.3) sediment	1.96	OSZ 1610	–	15020 ± 860	–
	TB-1 (2.0–2.3) sediment	2.28	OSZ 1614	–	19840 ± 1120	–
	TB-1 (2.0–2.3) snail	2.41	DeA-7448	19521 ± 73	23210–23790	11.7
	TB-3 (1.6–2.3) snail	2.45	DeA-7555	16991 ± 51	20300–20670	11.2

	TB-3 (2.6–3.0) sediment	2.81	OSZ 1611	–	23920 ± 1290	–
	TB-3 (3.5–3.75) sediment	3.62	OSZ 1612	–	23290 ± 1780	–
	TB-1 (3–3.2) sediment	3.68	OSZ 1615	–	19080 ± 1030	–
<i>Border of Silty and Clayey-silt layer (mean depth: 8.00 ± 1.0 m)</i>						
Clayey-silt footwall layer (S3)	TB-4 (8.4–8.8) peat	9.43	DeA-4676	27950 ± 296	31200–32650	46.5
	TB-1 (8.1–8.5) macrophyte	9.48	DeA-4670	26028 ± 269	29570–30840	43.1
	TB-5 (8.6–8.7) charcoal	9.57	DeA-4719	23073 ± 182	27040–27690	53.1
	TB-4 (10.8–11.0) shell (<i>Unio sp.</i>)	11.71	DeA-7556	32697 ± 157	36180–37220	11.3
	TB-3 (12.3–12.4) snail	11.81	DeA-7557	31173 ± 142	34700–35420	11.6
	TB-1 (16.6–16.9) charcoal	16.81	DeA-4672	36898 ± 353	40780–42050	53.7
	TB-1 (16.6–16.9) snail (<i>Gyraulus sp.</i>)	16.81	DeA-4518	> 40000	–	10.3
<i>Border of Clayey-silt and Sandy layer (S4) (mean depth: 18.50 ± 0.4 m)</i>						

*Relative position in the synthetic sequence/core (m); it corresponds to the relative depth of the sample in its actual lithostratigraphic layer in the actual core (actual depth of the sample in the layer divided by total thickness of the actual lithostratigraphic layer). Order of samples is defined by the relative position of the sample in the actual lithostratigraphic layer (TB-1 to TB-5). The “H-high” fraction means charred C fraction of the soil, combusted and extracted at 800°C.

^aThe radiocarbon ages are calibrated using the IntCal20 calibration (Reimer et al. 2020) and the OSL ages are the ages as explained in the text.

^xThe present surface (recent top meadow soil) represents the present-day (zero age) soil. The mean conventional apparent radiocarbon age of SOC H-fraction of the recent surface samples (940 ± 420 years, n = 5) was used to compensate the radiocarbon reservoir effect before calendar age calibration in case of deeper/older soil horizons.

(known as partial bleaching), which in turn can lead to age overestimation (Rittenour 2008; Tóth et al. 2017). The problem is especially significant for fine grained silty deposits. As earlier research near the Lower Tisza River has shown, the mean age-overestimation in case of fine-grained sediments can be ~ 1.5 kyrs in comparison to more reliable coarse-grain derived ages (Sipos et al. 2016). In this study we had opportunity to compare the obtained OSL data to overlying ^{14}C sample ages, which helped to create a more realistic combined method age-depth model. Unfortunately, in the case of these samples, there was no chance to separate coarse grains, thus we were not able to perform coarse-grain or comparative measurements using OSL.

The preparation of samples followed usual laboratory techniques (Mauz et al. 2002). All procedures were carried out in subdued yellow light provided by low pressure Na-lamps. Water content was determined using the formula of $(m_w - m_d)/m_d$, where m_w and m_d are wet and dry weight of the sample, respectively. We applied in situ water contents during the calculations and a $\pm 5\%$ error, which is sufficient in this floodplain environment with an almost continuous groundwater supply.

We attempted to separate grains as coarse as possible, but as the sampled sediments were silty deposits, the fine grain technique was applied, using the 11–20 μm fractions, or 4–11 μm in the case of two samples (OSZ1415, OSZ1416) which were separated by settling. Carbonates and organic material were removed by repeated treatment in 10% HCl and 10% H_2O_2 . The abundance of quartz in the samples was enhanced by a 7-day etching in H_2SiF_6 . Several aliquots of the same OSL samples were prepared by pipetting 2 mg of sample in suspension on aluminium discs.

OSL ages are calculated from the ratio of 1) the absorbed total dose (palaeodose or its laboratory equivalent), recorded by the amount of trapped charge, and 2) dose rate, the annual amount of radioactive dose to the mineral grains. OSL measurements themselves aim to determine the amount of absorbed dose by generating a function between laboratory doses and subsequent luminescence responses (dose response curve) (Figure S1). To determine the value of the absorbed total dose (D_e : equivalent dose) a RISØ DA-20 TL/OSL type luminescence reader was used (Bøtter-Jensen et al. 2010) and the single-aliquot regeneration (SAR) protocol was applied (Murray and Wintle 2003). Stimulation was carried out using blue (470 nm) LEDs, while detection was made through a U-340 filter. The suitability of the samples for dating was tested by comparing decay curves to that of the RISØ calibration quartz (Figure S1) and by performing dose recovery tests at different preheat temperatures (Figure S2). Although signal intensity was lower in case of the Tiszasüly samples, the decay curves fitted well to the standard, referring to adequate signal composition (Figure S1). Based on the dose recovery tests, the mean ratio of given and measured doses was close to unity (1.02 ± 0.01), while recycling ratios and recuperation values were also within the acceptable range (Figure S2). The IR/OSL ratio inserted at the end of the measurements showed that none of the samples contained any feldspar contamination.

Finally, SAR measurements were performed using 200°C/160°C preheat/cutheat treatment on 12 aliquots per sample. Dose points were fitted with a single-saturating exponential function. Standard rejection criteria (Murray and Wintle 2000; Duller 2003) were used to select aliquots for further calculations (recycling ratio: 1.00 ± 0.10 ; maximum dose error: 10%; maximum recuperation: 5%, maximum IR/OSL depletion ratio: 5%). Sample D_e was given as the mean and standard error of single-aliquot D_e values. Values were plotted on abanico plots (Dietze et al. 2016) (Figure S3) generated in the R luminescence package (Kreutzer et al. 2012).

Environmental dose rate (D^*) was determined by using high-resolution, extended range gamma spectrometry (Canberra XtRa Coaxial Ge detector), using 500 cm^3 marinelli beakers. Dry dose rates were calculated using the conversion factors of Adamiec and Aitken (1998). Effective α dose rate was calculated by using a 0.04 ± 0.02 a-value (Mauz et al. 2006). Attenuation factors for α and β dose rates were given after Brennan et al. (1991) and Brennan (2003), respectively. Wet dose rates were assessed on the basis of in situ water contents (Aitken 1985). The rate of cosmic radiation was based on burial depth following the equation of Prescott and Hutton (1994). The OSL ages have a relative error of 5–6%, which is reasonable in terms of fine grains ages, which provide an even distribution of equivalent doses.

3.4 Radiocarbon sample preparation and measurements

Most organic samples, for example plant fragments, charcoal and peat, were treated using the standard acid-base-acid (ABA) method, following standard protocols (Jull et al. 2006). The samples were treated with a sequence of 1N HCl, deionized (18 M Ω pure) water, 1M NaOH, deionized water, and then 1N HCl. For bulk soil and sediment samples, only the acid treatment was used. After the final acid wash, bulk samples were washed again with deionized water to slightly acidic pH (5–6) and then dried. Samples were then ready for two-stage combustion in oxygen and a final combustion with MnO₂.

For combustion and CO₂ purification, the Hertelendi Laboratory of Environmental Studies (HEKAL) AMS laboratory uses an in-line combustion and CO₂ purification line built in-house and based on system at the University of Arizona (Jull et al. 2006; Molnár et al. 2013a). Two-stage heating with controlled temperatures (400°C, “L-low” and 800°C, “H-high” fraction) is required to perform precise temperature-stabilized gradual fractional oxidation. Samples are combusted in the presence of 5.0 quality oxygen gas (Linde Hungary Ltd.). The carbon dioxide is cryogenically separated from water at –78°C using a mixture of isopropyl alcohol and dry ice, passed over Cu/Ag to reduce nitrogen oxides and remove halogens, and trapped in a known volume at liquid nitrogen temperature. The gas pressure is measured in a known volume, to calculate the yield. The combustion of the samples takes place in quartz tubes. On average, ~10 mg of a charcoal sample and ~1 g of soil or sediment were combusted. Then, the purified CO₂ gas sample is transferred to a sealed tube for graphitization. In the case of snails and shells, the samples were placed in a two-finger flask with a special valve. Samples were placed in the standing finger and the phosphoric acid in the other. After evacuating the flask, the acid (85% H₃PO₄ aq) is poured onto the sample in the other finger. The CO₂ produced from the carbonate in the sample is then introduced into our on-line combustion/CO₂ purification system (Molnár et al. 2013a).

The last step of the sample preparation in most cases is the graphite production from the CO₂ gas samples. Graphite targets were prepared by a sealed tube graphitization method at HEKAL (Rinyu et al. 2015). After transfer of the CO₂ gas and sealing of the reaction tubes, the graphitization process consists of 2 steps: 1) 3 hr at 500°C to release the hydrogen and reduce the iron powder, and 2) 5 hr at 550°C regular graphitization process.

All of the ¹⁴C measurements reported below were performed by our EnvironMICADAS AMS (Molnár et al. 2013b). Measurement time and conditions were set to collect at least 200,000 net counts for every single target in case of a modern sample. The overall measurement uncertainty for a modern sample is <3%, including normalization, background subtraction, and counting statistics. For testing organic sample preparation procedures, the laboratory used international ¹⁴C reference materials with known ¹⁴C activity (IAEA-C9 [wood]), and carbonate samples IAEA-C1 (marble) and IAEA-C2 (travertine).

Furthermore, we can simultaneously measure the ¹³C/¹²C ratio of the sample, which is essential for the correction of the radiocarbon age. The maximum age of ¹⁴C measured with this instrument is 50,000 years and the average measuring time of each sample is approximately half an hour (Molnár et al. 2013b). The blank level for each type of samples in case of 1 mg C carbon content is very reproducible around 0.3–0.5 pMC. The results are quoted as conventional radiocarbon ages in years BP (Table 2).

3.5. Age-depth model construction

To explore the history of the past 40,000 years for this research area, we have summarized the ¹⁴C and OSL data into an integrated age model, also taking into account the different bed thicknesses in each borehole. In the following, we present the age-depth model of the integrated “synthetic” cores using the BACON software package (Blaauw and Christen 2011). We have interpreted the information provided by each sample as a function of the environmental and climatic conditions that—according to the literature—may have been associated with that period. In the integrated age-depth model, the apparent age-corrected and calibrated ¹⁴C and OSL ages were used together as two independent age indicators.

Although the radiocarbon method is more applicable to short-lived organic matter (wood, charcoal, plant residues, gastropods, bivalve) than dating bulk soil, we have obtained a consistent depth model for the three genetic levels.

The ^{14}C and OSL data from the 5 boreholes were transferred into a uniform age model, taking into account the different layer thicknesses per borehole. Age-depth modelling calculation was obtained using Bayesian age modelling software BACON (Blaauw and Christen 2011) version 3.2 with the IntCal20 calibration curve (Reimer et al. 2020). The age-depth model was separated into three sections (S1-S2-S3) based on specific periods (see Figures 4–6 and Section 4).

4. Results and Discussion

4.1 Results of radiocarbon and OSL analyses

In Table 2. conventional and calibrated radiocarbon ages (yr BP/cal BP) and OSL (yr before 2019) data with the material types (SOC, sediment, snail, gastropod, macrophyte, peat, charcoal) and depths. In total, 29 ^{14}C ages and 8 OSL ages were obtained from the 5 investigated cores.

Although the OSL signal of the Tisza flood plain samples was weaker than for the calibration quartz standard, their decay curves are similarly shaped and indicate that the OSL signal is dominated by the fast component. Based on the dose recovery tests, the mean ratio of measured and regenerated doses was close to unity (1.02 ± 0.01), while recycling ratios and recuperation values were also within the acceptable range.

Some of the intact snail samples revealed in parallel drill cores have also been identified by species, namely *Pupilla sp.* (terrestrial gastropod) (TB-2 [2 m] and TB-4 [1.5–1.7 m]) these were in layer S2; while *Gyraulus sp.* (aquatic gastropod) (TB-1 [16.6–16.9 m]) and a *Unio bivalve* (TB-4 [11 m]) in layer S3. Macrophytes and charcoal remains were also recovered from the S3 layers at 8.1–8.5 m (TB-1), 8.6–8.7 m (TB-5). From the sedimentological point of view, the yellow, silty-clay layer (a carbonate-sulphate complex) indicates that the area has started to become land-based at this time. Occasionally, during small floods, the sediment-surface must have been inundated or at least partially saturated with water, as evidenced by the appearance of redox spots (Fe-Mn mottles). However, *Pupilla sp.* was found at 2 m depth (DeA-7449, 20380 ± 77 BP, $24215\text{--}24850$ cal BP), falling into the Last Interstadial which was a warmer climate period and preceded the Last Glacial Maximum (iSBLGM, 23000–25000 kyrs [after Gábris 2003]). *Unio sp.* (DeA-7556, 32697 ± 157 , $36180\text{--}37220$ cal BP) and *Gyraulus sp.* (DeA-4818, > 40000 BP) were found much deeper in the TB-1 borehole profile. The habitat of both species is aquatic, which is supported also by the type of the sediment, indicating an environment fostering the accumulation of gray clayey-silt (S3). In terms of climate, these sediments must have been deposited at the time of the Denekamp (34–36 kyrs) and Hengelo (38–40 kyrs) interstadials (after Gábris 2003).

In all cases, the ^{14}C measurements of the snail shells collected from the 5 boreholes in this area gave increasing “snail ages” that were consistent with the nature of the sediment and the former depositional environment. Overall, there was no significant “limestone effect,” charcoal and snail samples (TB-1 16.6–16.9 m) from nearly the same depth intervals gave similar results.

In earlier examples in the literature, the so-called limestone or “hard-water”-effect should be considered in the radiocarbon data of snails (Újvári et al. 2014). Snails may, namely, carry older “fossil,” limestone-sourced CaCO_3 and incorporate it into their skeleton, thus modifying their real age. Previous studies have documented that land snail shells yield anomalously old radiocarbon ages reaching as much as 3000 yrs offset due to incorporation of old, ^{14}C -free carbonate from the local substrate into shell carbonate. This phenomenon is often referred to as the “limestone problem” (Evin et al. 1980; Goodfriend 1987; Goodfriend and Hood 1983; Goodfriend and Stipp 1983; Rubin et al. 1963; Tamers 1970; Xu et al. 2011; Yates 1986; Zhou et al. 1999).

Table 3. Summary table of age interval and app. accumulation rate of the different layers of the “synthetic core”

Sediment layers/sections	S1	S2	S3
Corresponding climatic section	Holocene	LGP/UPG	MPG
Duration (kyr)	0–10.0	19.1–32.9	27.7–45.1
Depth interval (m)*	0–1.0	1.0–8.0	8.0–17.0
Thickness (m)	1.0	7.0	9.0
ap. Acc. Rate (aAR) (yr/cm)	100	20	19

*abs. distance from the top recent surface (m), aAR: apparent accumulation rate. LGP: Last Glacial period, UPG: Upper Pleniglacial, MPG: Middle Pleniglacial

4.2 Age-depth model and associated climatological aspects

Out of the 5 parallel drill cores, a total of 37 age results were obtained, 29 ^{14}C (blue symbols) and 8 OSL (light green symbols) results were included in the model (Figure 4). The model also attempted to estimate the history of accumulation of the sedimentary sequence over time (Table 3).

The obtained radiocarbon age data (cal BP 2σ) were fit into the local age-climate subdivision of the Late Pleistocene–Holocene published by Gábris (2003) and Gábris and Nádor (2007); modified by Cserkés-Nagy. (2013) after Sümegi and Krolopp (2002). We interpreted the results of the studied sequences in this framework (Figure 4).

Given known Late Quaternary climatic fluctuations, it was expected that the traces of extreme climatic conditions would also appear in the strata of the research area, and that traces of these temporary variations would be preserved in the layers.

We assumed that a *hiatus* might occur at the borders between S1-S2 or S2-S3 layers. As it is presented in (Figure 4) a significant *hiatus* was detected, indeed, between layers S1-S2. The detailed description of the time interval of this break at the border of S1-S2 in the age-depth model is discussed below.

4.2.1 Recent top meadow soil (S1: A, B, C)—the Holocene

According to our age-depth model, the formation-times of the meadow soil samples taken from 3 levels (top-middle-bottom) all fall into the Holocene (Figure 5).

These samples represent the upper 0–1.1 m layer of the five drill cores tested. The soil organic matter (SOC H-fraction) of the present surface (recent top meadow soil) of each individual core was dated by ^{14}C and their conventional apparent radiocarbon age was used for reservoir correction on the core. The mean apparent age of the five cores was 940 ± 420 years ($n = 5$), which is in good agreement with earlier soil apparent age observations from the Carpathian Basin (Buró et al. 2019; Molnár and Svingor 2011; Novák et al. 2018; Tóth et al. 2018). The apparent radiocarbon age of the core was used to correct the radiocarbon reservoir effect on the deeper buried soil layers measured by the same method on the SOC H-fraction. The reservoir-corrected soil organic matter ages were used in the BACON model to calculate the synthetic age-depth sequence (Figure 5).

We have applied the “apparent age” correction only to samples that are mostly Holocene. One has to be very careful on the impact of using a correction of “recent soil mean apparent ^{14}C age” to define the age of older soils or older horizons. It could be an extra error generated by not taking into account the evolution of atmospheric ^{14}C history, and give significant contribution for the associated error (100–150 ^{14}C years) if not exactly calculated. As dynamics of upper horizons is not the dynamics of lower horizons.

This consolidated Holocene section (S1) is about 1.0–1.1 m thick and shows ~ 100 yr/cm apparent mean accumulation rate, based on five investigated sequences (Table 3). According to the model the S1 layer began 10.0 kyr ago, although we have observed some few thousand years older ages, too,

(both ^{14}C and OSL) in some individual cores (SOC H-fraction ^{14}C : TB-4 [1.0–1.2] and TB-1 [1.0–1.2], sediment OSL: TB-1 [1.0–1.2]).

There are 16 age data available to describe the 1 m thick section, which comes from 5 different boreholes and of course, due to the uncertainty arising from the methodological limitations of age determination and the model, we obtained an imperfectly consistent age model. It seems obvious that this layer covers the entire Holocene from 10 kyrs cal BP to present.

At the bottom of the S1 close to the S2 layer, gypsum and sulphate precipitation, as well as CaCO_3 concretions appear in the meadow soil, which typically occur in arid/semi-arid climate conditions.

4.2.2 Silty-clay layer (S2)—Last Glacial to Upper Pleniglacial

Looking at the boundary between the Meadow soil (S1) and Silty-clay layer (S2) (mean depth: 1.02 ± 0.2 m) in some individual cores (TB-2 and TB-3), the ^{14}C age of the neighbouring layers have significant age steps in a relatively short depth distance. The apparent mean accumulation rate jumps from 20 yr/cm to 100 yr/cm at the border (Table 3).

According to the BACON age-depth model, it is likely that significant amounts of the sediment are missing at the boundary between S1 and S2 namely from the period between 10 to 19 kyrs cal BP. This means that the upper part of layer S2 finished at 19 kyrs cal BP while S1 layer starts only at 10 kyrs cal BP.

In the literature there are very similar *hiatuses* at this age range (between 10 and 24 kyrs cal BP) just below the recent top soil layer at the Dunaszekcső loess sequence and also at the Süttő loess sequence (Novothy et al. 2011; Újvári et al. 2016). At Dunaszekcső, the recent top soil is 2.3 m thick and the loess layer ends at this 2.3 m depth while its age at the top is about ~ 24 kyrs. It means there is a *hiatus* between 12 and 24 kyrs in the sequence at the Dunaszekcső. At Süttő, we have constructed a BACON age-depth model for the top loess layer (depth 0.66–6.00 m), using the reported OSL ages from Novothy et al. (2011). The model output shows the top part of the loess layer was formed about ~ 24.3 kyrs ago (Figure S4). There is only a relatively thin top recent soil above this loess sequence (66 cm thick), which is formed very likely during the Holocene. Thus, also for the Süttő loess sequence there is a *hiatus* for the age period between 12 and 24 kyrs cal BP.

According to the regional climatic- and environmental change characteristics (environment and climate construction) established by Gábris and Nádor (2007), Gábris and Nagy (2005), Gábris et al. (2012), and Kasse et al. (2010) for the Upper Pleistocene and Holocene periods, the *hiatus* encompasses the very beginning of the Holocene and the Late Glacial and Upper Pleniglacial periods. Possible reason for the unconformity might be the wind erosion process as it is usually one of the main drivers of landform formation during cold-dry climatic periods. Wind erosion processes do not favor large-scale sediment accumulation in this region (Cserkész-Nagy 2013). At the beginning of the LGM (Last Glacial Maximum, 23–18 kyrs cal BP ago), the climate showed a tendency to gradually become drier and cooler, which was interrupted by periodic reliefs. The LGM across Europe ended 18–20 kyrs cal BP ago, which was followed by gradually warming periods in which warmer and colder periods alternated. The sedimentary hiatus period includes the Ságvár-Laxcaux interstadial (16.5–19 kyrs), the oldest Dryas (16.5–14.6 kyrs cal BP) and the entire period of the Late Glacial (14.6–11.6 kyrs cal BP), and the accepted beginning of the Holocene (preBoreal period, 11.6–10.2 kyrs cal BP) (Gábris and Nádor 2007).

The presence of the *hiatus* in the studied Tiszasüly sedimentary column between 10 to 19 kyrs cal BP reinforce the hypotheses of Gábris (2002, 2003), according to which during the Older Dryas and Ságvár-Laxcaux periods, there was an erosional event (significant meander-cutoff) at the Middle-Tisza region, which can be traced back to some regional climatic influence.

The S2 (depth: 1.0–8.0 m) layer belongs to the Late Glacial and Upper Pleniglacial periods (Figure 6). During these periods (LG/UPG), stadials and interstadials (cold-dry and warm-wet periods) frequently alternated. S2 covers the age range between 19 and 29.2 kyrs cal BP within a 7 m thick layer (depth between 1.02 to 8.0 m).

The S2 layer represents an area of dry land that has become a high flood plain, so continuous fluvial activity probably ceased at this point. From the point of view of sediment stratigraphy, this can be considered an aggrading flood-plain environment, when there were minor and major climate fluctuations during this time. With a sedimentation rate of 20 yrs/cm, it shows a much faster sedimentation than the formation of the S1 Holocene soil layer (100 yrs/cm aAR). But the formation of the S2 layer is twice as slow as the model-calculated value (10 yrs/cm) for the kiln during this period, as well as the accumulation rate of 10 years/cm reported for the loess sequence in Dunaszekcső.

The sediments qualify as a carbonate-sulphate-pedocal-solonetz type soil-sedimentary complex. Its unusual thickness can be explained by the aggradation of the flood plain.

4.2.3 Clayey-silt layer (S3)—Middle Pleniglacial

Based on the age-depth model, the formation of this section falls in the Middle Pleniglacial period. This 18.8 kyrs long period (between 29.2 to 48.0 kyr BP) of sedimentation resulted in deposits with a thickness of 10.5 m (depth between 8.0 to 18.5 m). This part of the section has a very similar accumulation rate as the S2 layer above it (19 yr/cm aAR) (Figure 6, Table 3).

According Gábris and Nagy (2005), at the end of the Middle Pleniglacial (conv. 29–60 ¹⁴C yrs BP), the warm-humid climate was the most characteristic with one stadial interruption. At that time, fluvial processes dominated the area, which resulted in high rate of sedimentation (Gábris and Nagy 2005).

The age-depth model results of S3 layer and its lithological features are in good agreement with the climatic events described above by Gábris and Nagy (2005) mentioned above. The S3 sediment layer has a laminated structure (settling of suspended load) and contains also peat, organic detritus, and a few goethitic spots. It may indicate that this part of the sedimentary sequence was deposited in a stagnant/“dead-” water environment. This layer was most likely formed as the filling material of an abandoned meander (oxbow) of the “Paleo-Bodrog.” The appearance of a peat layer in this section also indicates a stagnant/“dead”-water environment with anaerobic conditions. The presence of the anaerobic environment is also supported by the appearance of vivianite (an iron-phosphate mineral) in this layer.

Sandy intercalations and sand layer (S4) below the S3 layer, begin below 18.5 m depth, and their formation ages are much older than 40 kyr BP. As already mentioned, we did not study this part of the section in detail.

5. Conclusion

The evolution of river channels and flood plains over time has great significance in understanding environmental change. In flood-plain areas, the dynamics of landform formation may be more intense than in other areas.

According to earlier hypotheses, hundreds of meters of Quaternary sediments were deposited by the precursors of the present-day Tisza and Danube Rivers and their tributaries in the Great Hungarian Plain (Hungary). The Tizasüly research area, together with the whole Carpathian Basin, was part of the periglacial belt during glacial periods of the Pleistocene, so contiguous ice sheets covered the land surface only in the mountainous regions to the North. Rónai (1985) and Kuti and Kőrössi (1989) suggested that the Holocene sedimentation alone might have reached 30–40 m at the top of the sediment column in the Jászság Basin.

Obviously, during the last 40,000 years, sedimentation in this near-floodplain environment has had highly variable dynamics, and some major floods or other erosional effects may even have removed parts of the sequence. In the wider surroundings about 14–18 kyrs ago there might have been several meander-cutoffs until after the Tisza River finally shifted to its present position. The currently available age- and climatic data, suggest that in addition to the Paleo-Tisza and Paleo-Danube, there was also a third river, the “Paleo-Bodrog” of considerable water output, that might have existed in the past in this huge alluvial plain.

^{14}C and OSL results of five parallel, neighbouring cores were examined from a flood plain area (Jászság Basin 2.5–3 km away from the main channel of the river Tisza) in the Tisza River flood plain. Four major sedimentary layers (S1 to S4) were identified in all cores (S1: meadow soil; S2: silty-clay; S3: clayey-silt; S4: sand). The Solonetz-meadow type recent topsoil was sampled in three levels (at the modern surface (S1-A); at middle level (S1-B); and at the contact with the underlying yellow-coloured silty-clay [S1-C]) to gain a more detailed picture about the recent soil formation.

In total 29 ^{14}C (altogether 9 gastropods, 1 bivalve or shell-fragments, 1 sample of peat, 1 macrophyte, and 2 pieces of charcoal) ages and 8 OSL (from a depth of 3–3.5 m) ages were obtained from the 5 investigated cores. ^{14}C and OSL data were integrated into a “synthetic” age model using the BACON software package, taking into account also the different thicknesses of the layers encountered in each borehole.

Our results showed that the thickness of the Holocene deposits covering the older Pleistocene layers in the studied area is only 1.5–2 m (the entire S1 recent top meadow soil), instead of the 30–40 m estimated by previous authors (Kuti and Kőrössi 1989; Rónai 1985) for the Jászság Basin. The apparent mean accumulation shows an approximate rate of 100 yr/cm, based on five investigated sequences. After the S1 horizon, there is a sudden change to apparent accumulation rate (aAR: 20 yr/cm) in the S2 layer, indicating much faster sedimentation.

The silty-clay (S2) layer exhibits the following lithologically characteristics, reflecting the variable redox conditions of the floodplain environment: redox spots (Fe-Mn mottle). Some intact snail samples were also found in the sediment, namely *Pupilla sp.* (terrestrial gastropod) which typically refer to arid conditions. The S2 sediments can be considered as a carbonate-sulphate-pedocal-solonetz type soil sedimentary complex, the unusually large thickness (avg. 7 m) of which can be related to the former aggradation flood plain environment. The formation of the layer falls into the Last Glacial and Upper Pleniglacial climatic period.

Furthermore, the present study also supports the claims of Gábris (2002, 2003), according to which there must have been a major meander-cutoff (erosional event) after the Older Dryas and Ságvár-Lascaux. This event appears also in our BACON depth model (Figure 4) as a sudden slope change (at the boundary between S1-S2). Our age-depth model suggests that sediment is missing from the period between 10 to 19 kyrs BP in the Tizasüly sediment cores. In the literature, there are very similar hiatuses indicated at this age range (between 10 to 24 kyrs BP) in the Carpathian Basin, at the Dunaszekcső and also at the Süttő loess-paleosol sequence (Novothy et al. 2011; Újvári et al. 2016) when data are analysed from this point of view. We suggest therefore that this may be the sign of some important regional event.

The S3 (clayey-silt) layer is the thickest in the cores (9 m). It was formed during the Middle Pleniglacial climatic period, and its sedimentation rate is aAR: 19 yr/cm. The S3 deposit is presumed to have formed in a stagnant water environment, as indicated by its laminated structure (suspended load) and the presence of organic macrophytes, charcoal, *Gyraulus sp.*, and *Unio bivalve* (aquatic gastropod). Presumably, it was formed as the filling material of the former abandoned meander (oxbow) of the “Paleo-Bodrog.”

In addition to the obvious climatic control, the observed stratigraphic changes and the changes of sediment accumulation rate might be influenced also by tectonic movements having affected the Jászság Basin since Miocene times.

Our study delivered some new and important details about the surface evolution of the investigated Tizasüly area. New aspects of Holocene sedimentation and missing documents of an about 10 kyrs period was revealed using combined dating methods (^{14}C and OSL) on multiple cores.

Supplementary material. To view supplementary material for this article, please visit <https://doi.org/10.1017/RDC.2024.140>

Acknowledgments. The research was supported by the European Union and the State of Hungary, co-financed by the European Regional Development Fund in the project of GINOP-2.3.2-15-2016-00009 “ICER.” The work was also supported by the Hungarian National Research, Development and Innovation Office under grant No. NKFIH K 119309 and the Bolyai János Research Grant under No. BO/00451/17.

References

- Adamiec G and Aitken M (1998) Dose rate conversion factors: Update. *Ancient TL* **16**(2), 37–50.
- Aitken MJ (1985) *Thermoluminescence Dating*. Orlando/London: Academic Press, 351.
- Bertalan L, Rodrigo-Comino J, Surian N, Šulc Michalková M, Kovács Z, Szabó Sz, Szabó Gy and Hooke J (2019) Detailed assessment of spatial and temporal variations in river channel changes and meander evolution as a preliminary work for effective floodplain management. The example of Sajó River, Hungary. *Journal of Environmental Management* **248**, 109–277.
- Blaauw M and Christen JA (2011) Flexible paleoclimate age-depth models using an autoregressive gamma process. *Bayesian Analysis* **6**(3), 457–474.
- Borsy Z (1954) Geomorfológiai vizsgálatok a Bereg-Szatmári-síkságon. *Földrajzi Értesítő* **3**(2), 270–279.
- Borsy Z (1989) Az Alföld hordalékkúpjainak negyedidőszaki fejlődéstörténete. *Földrajzi Értesítő* **38**(3–4), 211–224.
- Borsy Z and Félégyházi E (1982) A vízhálózat alakulása az Alföld északi részében a pleisztocén végétől napjainkig. *Szabolcs–Szatmári Szemle* **3**, 23–32.
- Bøtter-Jensen L, Thomsen KJ and Jain M (2010) Review of optically stimulated luminescence (OSL) instrumental developments for retrospective dosimetry. *Radiation Measurements* **45**(3–6), 253–257.
- Brennan BJ (2003) Beta doses to spherical grains. *Radiation Measurements* **37**(4–5), 299–303.
- Brennan BJ, Lyons RG and Phillips SW (1991) Attenuation of alpha particle track dose for spherical grains. *International Journal of Radiation Applications and Instrumentation. Part D. Nuclear Tracks and Radiation Measurements* **18**(1–2), 249–253.
- Brock F, Froese GD and Roberts GR (2010) Low temperature (LT) combustion of sediments does not necessarily provide accurate radiocarbon ages for site chronology. *Quaternary Geochronology* **5**, 625–630.
- Buró B, Lóki J, Győri E, Nagy R, Molnár M and Négyesi G (2019) New radiocarbon data from the palaeosols of the Nyírség blown sand area, Hungary. *Radiocarbon* **61**(6), 1–13.
- Buró B, Sipos Gy, Lóki J, András B, Félégyházi E and Négyesi G (2016) Assessing Late Pleistocene and Holocene phases of aeolian activity on the Nyírség alluvial fan, Hungary. *Quaternary International* **425**, 183–195.
- Chichagova OA and Cherkinsky AE (1993) Problems in radiocarbon dating of soils. *Radiocarbon* **35**(3), 351–362.
- Crombè P, Strydonck van M, Boudin M, Brande van den T, Derese C, Vandenberghe AGD, Haute van den P, Picon-Court M, Verniers J, Gelorini V, Bos AAJ, Verbruggen F, Antrop M, Bats M, Bourgeois J, Reu DJ, Maeyer DP, Smedt DP, Finke AP, Meirvenne van M and Zwertvaegher A (2012) Absolute dating (^{14}C and OSL) of the formation of coversand ridges occupied by prehistoric hunter-gatherers in NW Belgium. *Radiocarbon* **54**(3–4), 715–726.
- Cserkés-Nagy Á (2013) Egy Tisza-völgyi pleisztocén folyó rekonstrukciója ultranagy felbontású szeizmikus szelvények alapján. Morfometriai elemzések a paleoklíma becsüléséhez. PhD értekezés, ELTE Ált. és Alk. Földtani Tanszék, Budapest, 140.
- Dietze M, Kreutzer S, Burow C, Fuchs MC, Fischer M and Schmidt C (2016) The abanico plot: Visualising chronometric data with individual standard errors. *Quaternary Geochronology* **31**, 12–18.
- Doetterl S, Berhe AA, Nadeu E, Wang Z, Sommer M and Fiener P (2016) Erosion, deposition and soil carbon: A review of process-level controls, experimental tools and models to address C cycling in dynamic landscapes. *Earth-Science Reviews* **154**, 102–122.
- Duller GAT (2003) Distinguishing quartz and feldspar in single grain luminescence measurements. *Radiation Measurements* **37**(2), 161–165.
- Emiliani C (1955) Pleistocene temperatures. *The Journal of Geology* **63**(6), 538–578.
- Evin J, Marechal J, Pachiaudi C and Puissegur JJ (1980) Conditions involved in dating terrestrial shells. *Radiocarbon* **22**(2), 545–555.
- Fábián Sz, Kovács J and Varga G (2000) Újabb szempontok hazánk periglaciális klímájához. *Földrajzi Értesítő* **49**(3–4), 189–204.
- Frányó F (1992) Magyarország negyedidőszaki üledékeinek vastagságtérképe. Térkép, méretarány= 1:500 000, MÁFI, Budapest.
- Gábris Gy (2002) A Tisza helyváltozásai. In Mészáros R, Schweitzer F and Tóth J (eds), *Jakucs László, a tudós, az ismeretterjesztő és a művész*. MTA FKI – PTE SzE kiadása, Pécs, 91–105.
- Gábris Gy (2011) A Zagyva-Tarna alföldi vízrendszerének kialakulása és fejlődése. *Földrajzi Közlemények* **135**(3), 205–217.
- Gábris Gy, Félégyházi E, Nagy B and Ruszkiczay Zs (2001) A Középső-Tisza vidékének negyedidőszak végi folyóvízi felszínfejlődése (Late Quaternary Evolution of the Middle Tisza Region). I. MFK (Földrajzi Konferencia), Szeged, 1–10.
- Gábris Gy, Horváth E, Novothny Á and Ruszkiczay-Rüdiger Zs (2012) Fluvial and aeolian landscape evolution in Hungary—Results of the last 20 years research. *Netherlands Journal of Geoscience* **91**, 111–128.
- Gábris Gy and Nádor A (2007) Long-term fluvial archives in Hungary: Response of the Danube and Tisza rivers to tectonic movements and climate changes during the Quaternary. *Quaternary Science Reviews* **26**, 2758–2782.
- Gábris Gy and Nagy B (2005) Climate and tectonically controlled river style changes on the Sajó-Hernád alluvial fan (Hungary). In: Harvey AM, Mather AE and Stokes M (eds), *Alluvial Fans: Geomorphology, Sedimentology, Dynamics*. Geological Society of London, Special Publication 251(1), 61–67.
- Gábris Gy, Telbisz T, Nagy B and Belardinelli E (2002) A tiszai hullámtér feltöltődésének kérdése és az üledékképződés geomorfológiai alapjai. *Vízügyi Közlemények* **84**(3), 305–322.
- Gábris Gy (2003) A földtörténet utolsó 30 ezer évének szakaszai és a futóhomok mozgásának főbb periódusai Magyarországon. *Földrajzi Közlemények* **127**(51), 1–14.
- Goodfriend GA (1987) Radiocarbon age anomalies in shell carbonate of land snails from semi-arid areas. *Radiocarbon* **29**(2), 159–167.

- Goodfriend GA and Hood DG (1983) Carbon isotope analysis of land snail shells: Implications for carbon sources and radiocarbon dating. *Radiocarbon* **25**(3), 810–830.
- Goodfriend GA and Stipp JJ (1983) Limestone and the problem of radiocarbon dating of land-snail shell carbonate. *Geology* **11**(10), 575–577.
- Hales TC, Scharer KM and Wooten RM (2012) Southern Appalachian hillslope erosion rates measured by soil and detrital radiocarbon in hollows. *Geomorphology* **138**(1), 121–129.
- Harrison GK (1996) Using bulk radiocarbon measurements to estimate soil organic matter turnover times. *Radiocarbon* **38**(2), 181–190.
- Hemingway DJ, Rhtman HD, Grant EK, Rosengard ZS, Eglinton IT, Derry AL and Galy VV (2019) Mineral protection regulates long-term global preservation of natural organic carbon. *Nature* **570**(7760), 228–231.
- Horváth E, Bradák B, Novothny Á and Frechen M (2007) A löszök paleotalajainak rétegtani és környezetrekonstrukció jelentősége. *Földrajzi Közlemények* **131**(4), 389–406.
- Horváth F, Bada G, Windhoffer G, Csontos L, Dombrádi E, Dövényi P, Fodor L, Grenczy Gy, Síkhegyi F, Szafián P, Székely B, Timár G, Tóth L and Tóth T (2006) A Pannon-medence jelenkori geodinamikájának atlasza: Euro-konform térképsorozat és magyarázó. *Magyar Geofizika* **47**(4), 133–137.
- Horváth F and Tari G (1999) IBS Pannonian Basin project: A review of the main results and their bearings on hydrocarbon exploration. In: Durand B, Jolivet L, Horváth F and Séranne M (eds), *The Mediterranean Basins: Tertiary Extension within the Alpine Orogen*. Geological Society, London, Special Publications **156**, 195–213.
- Jámor Á (2002) A magyarországi éleskavics előfordulások és földtani jelentőségük. *Földtani Közlöny* **132**(különszám), 101–116.
- Joó I (1992) Recent vertical surface movements in the Carpathian Basin. *Tectonophysics* **202**, 129–134.
- Jull AJT, Burr GS, Beck JW, Hodgins GWL, Biddulph DL, Gann J, Hatheway AL, Lange TE, Lifton NA (2006) Application of accelerator mass spectrometry to environmental and paleoclimate studies at the University of Arizona. *Radioactivity in the Environment* **8**(21), 3–23.
- Kasse C, Bohncke SJP, Vandenbergh J and Gábris Gy (2010) Fluvial style changes during the last glacial-interglacial transition in the middle Tisza valley (Hungary). *Proceeding of the Geologists' Association* **121**(2), 180–194.
- Kiss T, Sipos Gy, Mauz B and Mezósi G (2012) Holocene aeolian sand mobilization, vegetation history and human impact on the stabilized sand dune area of the southern Nyírség, Hungary. *Quaternary Research* **78**(3), 492–501.
- Kiss T, Hernesz P, Sümegey B, Györgyóvics K and Sipos Gy (2015) The evolution of the Great Hungarian Plain fluvial system—Fluvial processes in a subsiding area from the beginning of the Weichselian. *Quaternary International* **388**, 142–155.
- Kretzoi M and Pécsi M (1982a) A Pannóniai-medence pliocén és pleisztocén időszakának tagolása. *Földrajzi Közlemények* **30**(4), 300–325.
- Kretzoi M and Pécsi M (1982b) Pleistocene and Quaternary chronostratigraphy and continental surface development of the Pannonian Basin. In: Pécsi M (ed), *Quaternary Studies in Hungary*, 11–42. MTA Földrajztudományi Kutató Intézet, Bp.
- Kreutzer S, Schmidt C, Fuchs MC, Dietze M, Fischer M and Fuchs M (2012) Introducing an R package for luminescence dating analysis. *Ancient TL* **30**(1), 1–8.
- Kuti L and Kőrössi L (1989) *Az Alföld Földtani Atlasza: Szolnok*. Magyar Állami Földtani Intézet, Budapest.
- Mauz B, Bode T, Mainz E, Blanchard H, Hilger W, Dikau R and Zöller L (2002) The luminescence dating laboratory at the University of Bonn: Equipment and procedures. *Ancient TL* **20**(2), 53–61.
- Mauz B, Packman S and Lang A (2006) The alpha effectiveness in silt-sized quartz: New data obtained by single and multiple aliquot protocols. *Ancient TL* **24**(2), 47–52.
- Miao X, Wang H, Hanson PR, Mason JA and Liu X (2016) A new method to constrain soil development time using both OSL and radiocarbon dating. *Geoderma* **261**(8), 93–100.
- Miháltz I (1967) A Dél-Alföld felszínközeli rétegeinek földtana. *Földtani Közlemények* **97**, 294–307.
- Mike K (1975) Utilization of the analysis of ancient river beds for the detection of Holocene crustal movements. *Tectonophysics* **29**(1–4), 359–368.
- Molnár M, Janovics R, Major I, Orsovsvki J, Gönczi R, Veres M, Leonard AG, Castle SM, Lange TE, Wacker L, Hajdas I and Jull AJT (2013a) Status report of the new AMS ¹⁴C sample preparation lab of the Hertelendy Laboratory of Environmental Studies (Debrecen, Hungary). *Radiocarbon* **55**(2), 665–676.
- Molnár M, Rinyu L, Janovics R and Major I (2013b) Az új debreceni AMS laboratórium bemutatása. *Archeometriai Műhely* **IX**(3), 147–160.
- Molnár M and Svingor É (2011) Radiokarbon kormeghatározás. *Régészeti kézikönyv* (CD). Magyar Régész Szövetség, Bp, 532–545.
- Munsell Soil Colour Charts (1990) *Soil Survey Manual*. U.S. Dept. Agriculture, Handbook, 18.
- Murray AS and Wintle AG (2000) Luminescence dating using an improved single-aliquot regenerative-dose protocol. *Radiation Measurements* **32**(1), 57–73.
- Murray AS and Wintle AG (2003) The single aliquot regenerative dose protocol: Potential for improvements in reliability. *Radiation Measurements* **37**(4), 377–381.
- Nádor A, Lantos M, Tóth Makk Á and Thamóné-Bozsó E (2003) Milankovich-scale multi-proxy records from fluvial sediments of the last 2.6 Ma, Pannonian Basin, Hungary. *Quaternary Science Reviews* **22**(20), 2157–2175.
- Nádor A, Thamóné-Bozsó E, Magyarai Á and Babinszki E (2007) Fluvial responses to tectonics and climate change during the Late Weichselian in the eastern part of the Pannonian Basin (Hungary). *Sedimentary Geology* **202**, 174–192.

- Nagy ÁT, Tóth T and Sztanó O (2007) A “harmadik folyó” — Pleisztocén folyóvízi üledékek ultranagy felbontású szeizmikus szelvényeken a Tisza Tiszadob-Martfű közti szakas
- Nagy ÁT, Tóth T and Sztanó O (2007) A “harmadik folyó” — Pleisztocén folyóvízi üledékek ultranagy felbontású szeizmikus szelvényeken a Tisza Tiszadob-Martfű közti szakaszán. *Földtani Közlöny* **137**(2), 239–260.
- Nagy ÁT, Vajk Ö, Tóth T and Sztanó O (2005) Természetes folyófejlődés a gátak közé szorított Közép-Tiszán. *Hidrologiai Közlöny* **85**(5), 55–62.
- Nian X, Zhang W, Wang Z, Sun Q, Chen J, Chen Z and Hutchinson MS (2017) The chronology of a sediment core from incised valley of the Yangtze River delta: Comparative OSL and AMS ¹⁴C dating. *Marine Geology* **395**, 320–330.
- Novák TJ, Molnár M and Buró B (2018) Reconstruction of soil carbon redistribution processes along a hillslope section in a forested area. *Radiocarbon* **60**(5), 1413–1424.
- Novothy Á, Frechen M, Horváth E, Wacha L and Rolf C (2011) Investigating the penultimate and last glacial cycles of the Süttő loess section (Hungary) using luminescence dating, high-resolution grain size, and magnetic susceptibility data. *Quaternary International* **234**(1), 75–85.
- Penck A and Brückner E (1901–1909) *Die Alpen im Eiszeitalter*. 3 vols. Tauchnitz, Leipzig, 0–1199.
- Prescott JR and Hutton JT (1994) Cosmic ray contributions to dose rates for luminescence and ESR dating: Large depths and long term variations. *Radiation Measurements* **23**(2–3), 497–500.
- Reimer PJ, Bard E, Austin WEN, Bayliss A, Blackwell PG, Bronk Ramsey C, Butzin M, Cheng H, Edwards RL, Friedrich M, Grootes PM, Guilderson TP, Hajdas I, Heaton TJ, Hogg AG, Hughen KA, Kromer B, Manning SW, Muscheler R, Palmer JG, Pearson C, van der Plicht J, Reimer RW, Richards DA, Scott EM, Southon JR, Turney CSM, Wacker L, Adolphi F, Büntgen U, Capano M, Fahrni SM, Fogtmann-Schulz A, Friedrich R, Köhler P, Kudsk S, Miyake F, Olsen J, Reinig F, Sakamoto M, Sookdeo A and Talamo S (2020) IntCal20 Northern Hemisphere radiocarbon age calibration curve (0–55 cal kBP). *Radiocarbon* **62**(4), 725–757.
- Rinyu L, Orsovski G, Futó I, Veres M and Molnár M (2015) Application of zinc sealed tube graphitization on sub-milligram samples using EnvironMICADAS. *Nuclear Instruments and Methods in Physics Research Section B: Beam Interactions with Materials and Atoms* **361**, 406–413.
- Rittenour TM (2008) Luminescence dating of fluvial deposits: Applications to geomorphic palaeoseismic and archaeological research. *Boreas* **37**(4), 613–635.
- Rónai A (1985) Az Alföld negyedidőszaki földtana. *Geologica Hungarica Series Geologica* **21**, 446.
- Rubin M, Likins RC and Berry EG (1963) On the validity of radiocarbon dates from snail shells. *The Journal of Geology* **71**(1), 84–89.
- Scharpenseel HW and Becker-Heidmann P (1992) Twenty five years of radiocarbon dating soils: Paradigm of erring and learning. *Radiocarbon* **34**(3), 541–549.
- Shackleton JN (1967) Oxygen isotope analyses and Pleistocene temperatures re-assessed. *Nature (London)* **215**, 15–17.
- Shackleton JN and Opdyke DN (1973) Oxygen isotope and palaeomagnetic stratigraphy of Equatorial Pacific Core V28-238: Oxygen isotope temperatures and ice volumes on a 105 year and 106 year scale. *Quaternary Research* **3**(1), 39–55.
- Shen HY, Yu LP, Zhang HM, Zhao M and Lai ZP (2015) OSL and radiocarbon dating of flood deposits and its paleoclimatic and archaeological implications in the Yihe River Basin, East China. *Quaternary Geochronology* **30**(PB), 398–404.
- Sipos Gy, Kiss T and Tóth O (2016) Constraining the age of floodplain levels along the lower section of River Tisza, Hungary. *Journal of Environmental Geography* **9**(1–2), 39–44.
- Stefanovits P, Filep Gy and Füleky Gy (1999) *Talajtan*. Budapest: Mezőgazda Kiadó, 470.
- Sümegey J (1944) *A Tiszántúl. Magyar tájak földtani leírása VI*. Magyar Királyi Földtani Intézet kiadása, 208.
- Sümegey P and Krolopp E (2002) Quaternary malacological analyses for modelling of the Upper Weichselian palaeoenvironmental changes in the Carpathian Basin. *Quaternary International* **91**, 53–63.
- Szabó J, Vass R and Tóth Cs (2012) Examination of fluvial development on study areas of upper-Tisza region. *Carpathian Journal of Earth and Environmental Sciences* **7**(4), 241–253.
- Tamers MA (1970) Validity of radiocarbon dates on terrestrial snail shells. *American Antiquity* **35**(1), 94–100.
- Tamm OC and Östlund GH (1960) Radiocarbon dating of soil humus. *Nature* **185**, 706–707.
- Thamóné-Bozsó E, Kercsmár Zs and Nádor A (2002) Tectonic control on changes in sediment supply on Quaternary alluvial systems, Körös sub-basin, SE Hungary. In Jones SL and Frostick LE (eds), *Sediment Flux to Basins: Causes, Controls and Consequences*. London: Geological Society, Special Publications **191**, 37–53.
- Timár G (2003) Földtani folyamatok hatása a Tisza alföldi szakaszának medermorfológiájára. ELTE, Doktori értekezés, 135.
- Timár G, Sümegey P and Horváth F (2005) Late Quaternary dynamics of the Tisza River: Evidence of climatic and tectonic controls. *Tectonophysics* **410**(1), 97–110.
- Tóth CsA, Prónay Zs, Braun M, Nagy P, Pethe M, Tildy P, Buró B, Kertész T, McIntosh RW and Molnár M (2018) Georachaeological study of Szálka and Vajda kurgans (Great Hungarian Plain) based on radiocarbon and geophysical analyses. *Radiocarbon* **60**(5), 1425–1437.
- Tóth O, Sipos Gy, Kiss T and Bartyik T (2017) Variation of OSL residual doses in terms of coarse and fine grain modern sediments along the Hungarian section of the Danube. *Geochronometria* **44**(1), 319–330.
- Trumbore ES (2000) Age of soil organic matter and soil respiration: Radiocarbon constraints on belowground C dynamics. *Ecological Applications* **10**(2), 399–411.

- Újvári G, Molnár M, Novothny Á, Páll-Gergely B, Kovács J and Várhegyi A (2014) AMS ^{14}C and OSL/IRSL dating of the Dunaszekcső loess sequence (Hungary): Chronology for 20 to 150 ka and implications for establishing reliable age-depth models for the last 40 ka. *Quaternary Science Reviews* **106**, 140–154.
- Újvári G, Molnár M and Páll-Gergely B (2016) Charcoal and mollusc shell ^{14}C -dating of the Dunaszekcső loess record, Hungary. *Quaternary Geochronology* **35**.
- Van Reeuwijk LP (1995) *Procedures for Soil Analysis*. International Soil Reference and Information Centre, Wageningen, 3rd ed.
- Vandenberghe J, Kasse C, Popov D, Markovic S, Vandenberghe D, Bohncke S and Gábris Gy (2018) Specifying the external impact on fluvial lowland evolution: The Last Glacial Tisza (Tisa) catchment in Hungary and Serbia. *Quaternary* **1**(2), 14.
- Vandenberghe J and van der Plicht J (2016) The age of the Hengelo interstadial revisited. *Quaternary Geochronology* **32**, 21–28.
- Wang Y, Amundson R and Trumbore S (1996) Radiocarbon dating of soil organic matter. *Quaternary Research* **45**(3), 282–288.
- Wiaux F, Vanclooster M, Cornelis JT and Van Oost K (2014) Factors controlling soil organic carbon persistence along an eroding hillslope on the loess belt. *Soil Biology and Biochemistry* **77**, 187–196.
- Xu B, Gu Z, Han J, Hao Q, Lu Y, Wang L, Wu N and Peng Y (2011) Radiocarbon age anomalies of land snail shells in the Chinese Loess Plateau. *Quaternary Geochronology* **6**, 383–389.
- Yates T (1986) Studies of non-marine mollusks for the selection of shell samples for radiocarbon dating. *Radiocarbon* **28**(2A), 457–463.
- Zhou W, Head WJ, Wang F, Donahue DJ and Jull AJT (1999) The reliability of AMS radiocarbon dating of shells from China. *Radiocarbon* **41**(1), 17–24.